NANO LETTERS

Letter

pubs.acs.org/NanoLett

Chiral Structure Determination of Aligned Single-Walled Carbon Nanotubes on Graphite Surface

Yabin Chen,[†] Yue Hu,[†] Mengxi Liu,[†] Weigao Xu,[†] Yanfeng Zhang,[†] Liming Xie,[‡] and Jin Zhang*[,†]

[†]Center for Nanochemistry, Beijing National Laboratory for Molecular Sciences, Key Laboratory for the Physics and Chemistry of Nanodevices, State Key Laboratory for Structural Chemistry of Unstable and Stable Species, College of Chemistry and Molecular Engineering, Peking University, Beijing 100871, China

[‡]Key Laboratory of Standardization and Measurement for Nanotechnology of Chinese Academy of Sciences, National Center for Nanoscience and Technology, Beijing 100190, China

Supporting Information

ABSTRACT: Chiral structure determination of single-walled carbon nanotube (SWNT), including its handedness and chiral index (n,m), has been regarded as an intractable issue for both fundamental research and practical application. For a given SWNT, the n and m values can be conveniently deduced if an arbitrary two of its three crucial structural parameters, that is, diameter d, chiral angle θ, and electron transition energy E_{ii}, are obtained. Here, we have demonstrated a novel approach to derive the (n,m) indices from the θ, d, and E_{ii} of SWNTs. Handedness and θ were quickly measured based on the chirality-dependent alignment of SWNTs on graphite surface. By combining their measured d and E_{ii}, (n,m) indices of SWNTs can be independently and uniquely identified from the (θ,d) or (θ,E_{ii}) plots, respectively. This approach offers intense practical merits of high-efficiency, low-cost, and simplicity.

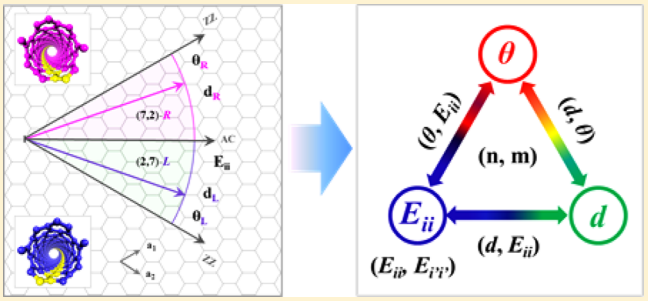

KEYWORDS: *Single-walled carbon nanotube, graphite, chirality determination, handedness, chiral angle, alignment*

Dramatic progress in the study of nanomaterials has benefitted greatly from sequential innovations in structural characterization methodology, especially in the case of low-dimensional carbon nanomaterials.[1,2] Single-walled carbon nanotube (SWNT),[3] a typical one-dimensional nanomaterial, is promising for many applications,[4−10] such as nanoelectronics, functional composites, and sensor devices. It is well-known that the superior properties of SWNTs sensitively depend on their unique chiral structures, including handedness and chiral index.[11] Therefore, chiral structure determination of SWNTs is absolutely essential to both fundamental research[12−15] and practical application.[8,16] Although much effort has been devoted to this daunting issue for two decades, as yet there is still lack of an efficient and accurate approach to comprehensively determine SWNT's chiral structures.

All current characterization techniques for the chiral structure determination of SWNTs can be principally divided into two categories: microscopies and spectroscopies. The microscopic techniques include scanning tunneling microscopy (STM),[17,18] high resolution transmission electron microscopy (HRTEM),[19,20] and selected-area electron diffraction (SAED).[21] Although these microscopic techniques can present the atomic structures of individual SWNT directly, they are all performed under rigorous conditions and at prohibitive costs. The spectroscopic techniques, based on the band structures of SWNTs, have played a pivotal role in the chirality determination of SWNT specimens, especially the abundance evaluation. Because of the Kataura-plot,[22] resonance Raman spectroscopy (RRS) has already been exploited to provide plentiful structure and property information of SWNTs,[23] however, it strictly requires continuous laser excitations to match the resonance window of each SWNT. In addition, photoluminescence excitation (PLE) is partially suitable for semiconducting SWNTs with small diameters,[24,25] and Rayleigh scattering spectroscopy (RSS)[26] is generally limited by the suspended structures of SWNTs. Furthermore, all spectroscopic techniques are unavailable to the handedness and chiral angle characterizations of SWNTs and are also seriously affected by the surrounding environmental factors of SWNT samples, such as temperature and dispersant. Thus, a convenient and accurate approach to fully determine chiral structures of SWNTs, especially handedness and chiral angle, is highly desirable.

Graphene, possessing similar conjugated structures to SWNT, has already been widely used to align SWNTs as an atomically smooth substrate.[27] Additionally, both theoretical and experimental results confirm that the orientation of aligned SWNT on graphene sensitively depends on its chirality, owing to their anisotropic interactions.[28] Ortolani L. et al. reported that the adhesion of SWNTs on graphene surfaces was

Received: September 6, 2013
Revised: October 18, 2013
Published: October 22, 2013

   dx.doi.org/10.1021/nl403336x | Nano Lett. 2013, 13, 5666−5671

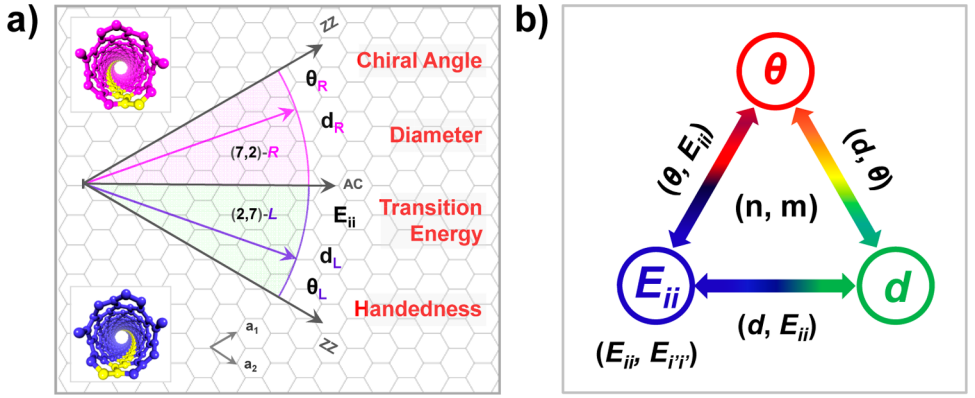

Figure 1. (a) Diagram of rolling graphene sheets into SWNTs with different chiral structures. The pink and blue sectors correspond to the right- and left-handed SWNTs, respectively. ZZ and AC refer to the zigzag and armchair edges of graphene, respectively. (b) Strategy for the chirality characterization of SWNTs. Using the θ, E_{ii}, and d of each SWNT, the approaches to (n,m) assignment can be divided into four types, including (θ,d), (d,E_{ii}), (θ,E_{ii}), and $(E_{ii},E_{i'i'})$.

chirality-dependent by HRTEM and SAED.[29] Moreover, our previous work[30] has also proven that the alignment of SWNT on graphene is highly chirality-selective. Herein, we report a rational approach to comprehensively determine chiral structures of aligned SWNTs on a graphite surface, using graphite trench as a critical reference. Detailed formulas were logically summarized to exactly measure chiral angle and handedness of SWNT. By further combining the obtained diameter and transition energy, the chiral index (n,m) of SWNTs can be uniquely assigned from the (θ,d) plot and (θ,E_{ii}) plot, respectively. This grand approach is suitable for rapid, cheap, and accurate characterizations of chiral structures of SWNTs on a large scale.

To develop a reliable and efficient characterization method, the inherent relationship between chiral index of SWNT and its intrinsic structures are crucially important. It is known that an SWNT could be conceptually described as a seamless cylinder of a rolled-up graphene sheet, and the rolling vector defined by (n,m) fully determines its diameter (d), handedness, chiral angle (θ), and electron transition energy (E_{ii}). For instance, the (7,2)-R and (2,7)-L (where R and L represent the zigzag right- and left-handednesses, respectively[31]) SWNTs are enantiomers with identical d = 0.64 nm and $\theta_R + \theta_L = 60°$ as shown in Figure 1a. Obviously, all structural characteristics of SWNT are mathematically correlated with the n and m values, that is, $d = a(n^2 + nm + m^2)^{1/2}\pi$ (a is the C−C length), $\theta = \tan^{-1}[((3)^{1/2}m)/(2n + m)]$ and $E_{ii} = f(n,m)$ (i is an integer). According to these expressions, the chiral index (n,m) can be logically deduced if any two parameters of d, θ, E_{ii}, or $E_{i'i'}$ (i and i' are different integers, which denote the van Hove transitions) are known. Following this strategy, approaches to the chirality assignment of SWNTs can be divided into four types, including (θ,d), (d,E_{ii}), (θ,E_{ii}), and $(E_{ii},E_{i'i'})$, as shown in Figure 1b. In this way, STM, HRTEM, and SAED of the microscopic techniques belong to the (θ,d) type based on the obtained atomic resolution images. RRS is typical of the (d,E_{ii}) type, owing to the radial breathing mode (RBM) shift and resonance energy.[23] RLE and RSS can simultaneously measure the different transition energies of isolated SWNTs,[25,26] which are typed in $(E_{ii},E_{i'i'})$. Obviously, the methods in the (θ,E_{ii}) type to determine (n,m) is still missing.

According to the above strategy, the (θ,d) plot, (d,E_{ii}) plot, (θ,E_{ii}) plot, and $(E_{ii},E_{i'i'})$ plot can be further proposed to simply identify the chiral indices of SWNTs; of these, the (d,E_{ii}) plot

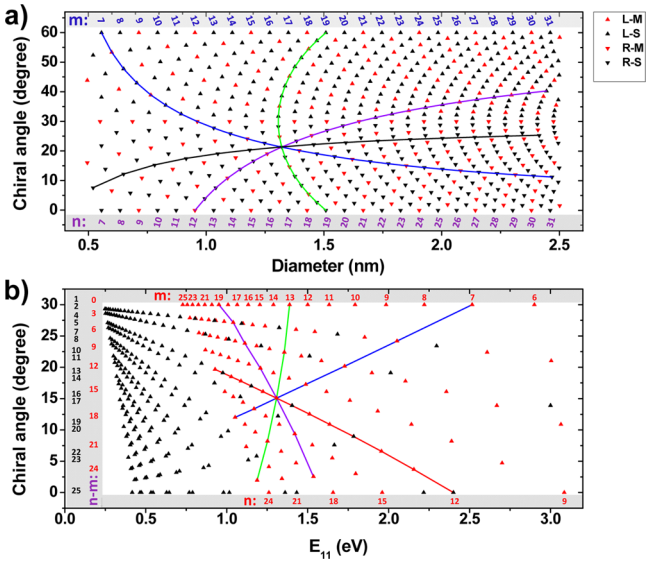

Figure 2. (a) The (θ,d) plot for chirality identification. (b) The (θ,E_{11}) plot for chirality identification. The upward-pointing, downward-pointing, red, and black triangles refer to the left-handed (L), right-handed (R), metallic (M), and semiconducting (S) SWNTs, respectively. The SWNTs on violet, blue, green, and black/red lines have the same n, m, $(n + m)$, and $(n - m)$ values, respectively.

and $(E_{ii},E_{i'i'})$ plot have already been extensively used for RRS and PLE. Figure 2a,b shows the (θ,d) plot and (θ,E_{ii}) plot (where i = 1, see Figure S1 in Supporting Information), respectively, which can provide abundant structure and property information of SWNTs, such as left-handed, right-handed, metallic, and semiconducting SWNTs. Moreover, the SWNTs on violet, blue, green, and black/red lines possess the same n, m, $(n + m)$, and $(n - m)$ values, respectively. Thus, the intersections of the four lines in the (θ,d) plot and (θ,E_{ii}) plot are (12,7)-R-S and (19,7)-R-M, respectively. Importantly, these two plots compensate for the disadvantage of Kataura-plot in that it is not well-suited for SWNTs with large diameters. Therefore, these useful (θ,d) and (θ,E_{ii}) plots are quite convenient for quickly identifying (n,m) of SWNTs. The determination of chiral angles is highly desirable for their realistic applications.

The chirality-dependent alignment of SWNTs on graphene surface shows the dominant advantages for their chiral angle

dx.doi.org/10.1021/nl403336x | Nano Lett. 2013, 13, 5666−5671

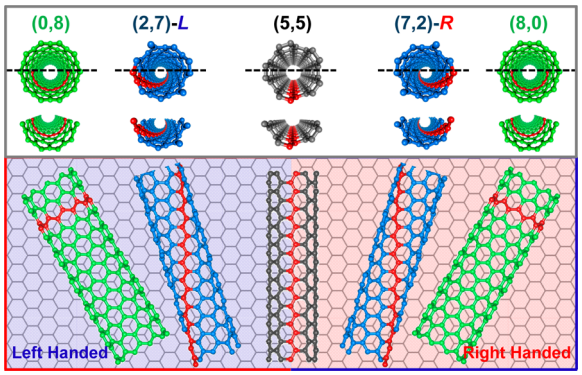

Figure 3. The anisotropic interactions between graphene and the aligned SWNTs with different chiral structures, including the zigzag (8,0) and (0,8) (green), armchair (5,5) (black), and chiral (2,7)-L and (7,2)-R (blue) SWNTs. The right- and left-handed SWNTs are distributed in the red and blue areas, respectively. The red carbon chains indicate the zigzag edges of SWNTs.

and handedness characterization.[30] The maximum interaction between a SWNT and graphite can be achieved if their interface has similar AB-stacking, which has already been fully proven by STM and HRTEM at an atomic scale.[29,30] The schematic in Figure 3 displays the stable configurations of graphene and SWNTs with different chiral structures. All SWNTs were artificially cut into two parts along their axial directions, and it is noticeable that all interfacial configurations are principally dominated by the lower parts of SWNTs. In this way, the orientations of zigzag (ZZ), armchair (AC), and chiral SWNTs in Figure 3 are aligned along the AC, ZZ, and chiral edges of graphene due to their own chiralities, respectively. In addition, the right- and left-handed SWNTs are only distributed in the red and blue areas, respectively. During the growth process of SWNT, many regular trenches along graphite ZZ edges can be frequently formed due to the etching effect of metal catalyst on a graphite surface,[32,33] which can be used for the handedness and chiral angle characterizations of aligned SWNTs on graphite.

Table 1. Approaches To Characterize the Handedness and Chiral Angle of Aligned SWNT on Graphite[a]

Handedness	$0^\circ < \varphi < 30^\circ$	$30^\circ < \varphi < 60^\circ$
R ($0^\circ < \theta < 30^\circ$)	$\theta = 30^\circ - \varphi$	$\theta = \varphi - 30^\circ$
L ($30^\circ < \theta < 60^\circ$)	$\theta = 30^\circ + \varphi$	$\theta = 90^\circ - \varphi$

[a]The dashed lines indicate the directions of the graphene trenches.

The handedness of SWNTs on graphene can be easily determined according to the relative positions of SWNTs and the zigzag orientated graphene trenches. As shown in Figure 4a, the right- and left-handed SWNTs are independently distributed in the 30° sectors (between the ZZ and AC edges of graphene) indicated by red and blue lines, and the graphene trenches can be randomly formed along either of the two ZZ directions. In this way, if a graphene trench appears in the

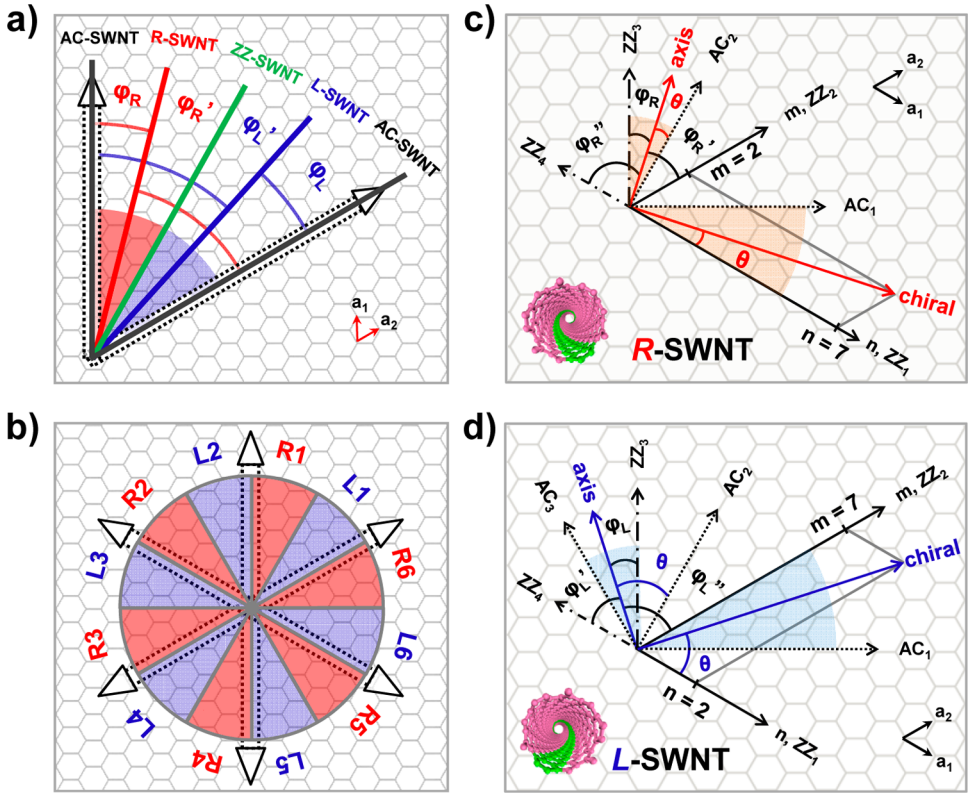

Figure 4. (a) Handedness determination of SWNTs. The black, red, green, and blue lines indicate the AC-SWNT, R-SWNT, ZZ-SWNT, and L-SWNT, respectively. (b) The distribution of right-handed (red sectors) and left-handed (blue sectors) SWNTs on graphene surface. The arrows in (a,b) indicate the zigzag edges of graphene. (c) Chiral angle determination of R-SWNT, with (7,2)-R as an example. (d) Chiral angle determination of L-SWNTs, with (2,7)-L as an example. The additional dotted and dotted-dashed lines indicate the AC and ZZ edges of graphene, respectively.

dx.doi.org/10.1021/nl403336x | Nano Lett. 2013, 13, 5666−5671

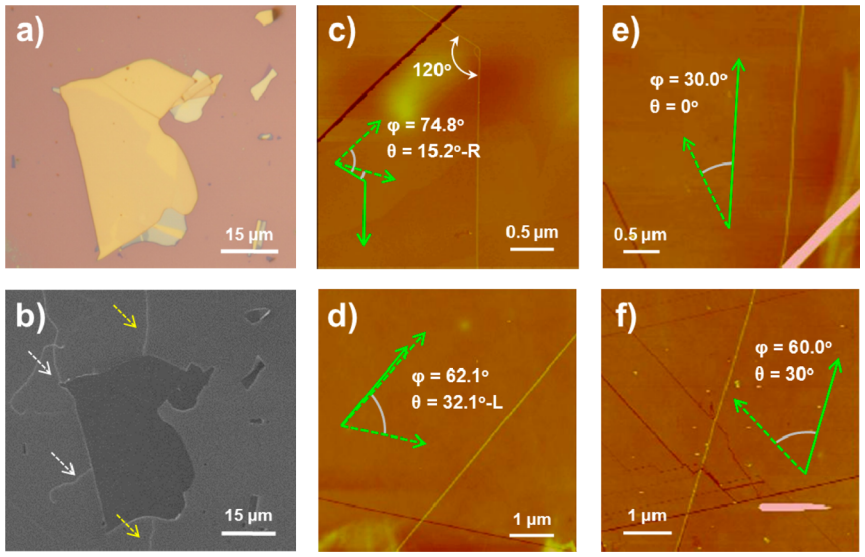

Figure 5. (a) Optical image of graphite substrate on SiO_x/Si surface. (b) SEM image of two grown SWNTs (indicated by arrows) on the same graphite surface. (c–f) The handedness and chiral angle characterizations of R-SWNT (c), L-SWNT (d), ZZ-SWNT (e), and AC-SWNT (f). The solid and dashed arrows indicate the directions of SWNT axes and the graphene trenches, respectively.

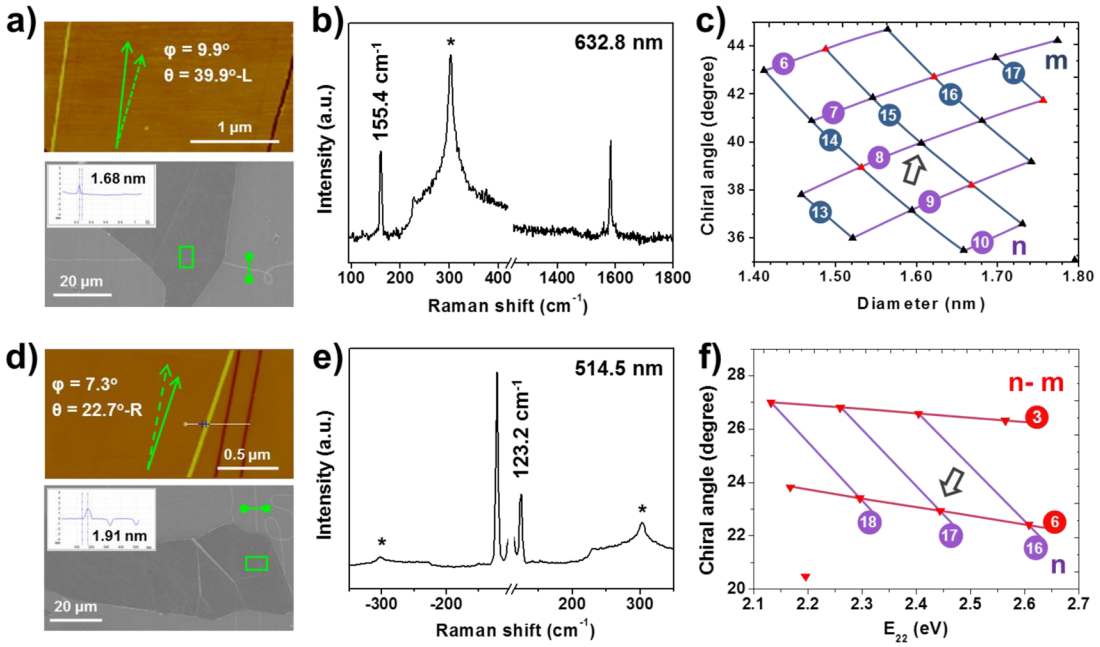

Figure 6. Chirality assignment of SWNTs using the (θ,d) plot and (θ,E_{ii}) plot. (a) AFM and SEM image of L-SWNT on a graphite surface. (b) Raman spectra of the SWNT on a silicon surface in (a). (c) The partial (θ,d) plot for the chirality assignment of SWNT in (a). (d) AFM and SEM image of R-SWNT on a graphite surface. (e) Stokes and anti-Stokes Raman spectrum of the SWNT on a silicon surface in (d). (f) The partial (θ,E_{22}) plot for the chirality assignment of SWNT in (d).

counter-clockwise (clockwise) direction of SWNT and the induced angle φ is $0° < \varphi_R < 30°$ ($30° < \varphi_R' < 60°$), then the SWNTs are right-handed. On the contrary, if a graphene trench appears in the clockwise (counter-clockwise) direction of SWNT, and the induced angle φ is $0° < \varphi_L < 30°$ ($30° < \varphi_L' < 60°$), then the SWNTs are left-handed. In addition, the angles between the achiral ZZ-SWNTs and AC-SWNTs, and the graphene trench are only 30 and 0°, respectively. Because of the D_{6h} symmetry of graphene, Figure 4a is only one of the six sectors, marked by R_1/L_1 to R_6/L_6, as shown in Figure 4b. As such, the handedness of SWNT can be easily determined by estimating its angle with the graphene trench.

The chirality-dependent alignment of SWNTs on graphene could also be exploited to easily characterize their chiral angle. The handedness determination of SWNT is a prerequisite for the chiral angle calculation. It is well-known that the chiral angles of ZZ-SWNT and AC-SWNT along the AC and ZZ edges of graphene are 0 and 30°, respectively. To a R-SWNT distributed in the red area in Figure 4c, such as (7,2)-R, the chiral angle θ between the chiral vector and the ZZ_1 edge of graphene is equivalent to the angle between its axial direction and AC_2 edge of graphene. If the graphene trench appears along the ZZ_3 (ZZ_2) edges, and the formed angle with SWNT axis is φ_R (φ_R'), the chiral angle of R-SWNT is $\theta = 30° - \varphi_R$ (θ

dx.doi.org/10.1021/nl403336x | Nano Lett. 2013, 13, 5666–5671

Table 2. Possible Chiral Structures (Handedness, Chiral Angle, and Chiral Index) of Aligned SWNTs on a Graphite Surface Predicted by the (θ,d) Plot

φ (°)	θ (°)		Handedness	ω_{RBM} [a]	d (nm)			(n,m)
	expt.	calc.	(R/L)	(cm^{-1})	ω_{RBM}	AFM	calc.	
9.9	39.9	40.0	L	155.4*	1.60	1.68	1.58	(8,15)
81.1	51.1	51.1	L	168.3*	1.48	1.39	1.31	(3,15)
3.5	26.5	26.6	R	125.7*	1.98	2.05	1.97	(16,13)
7.3	22.7	23.0	R	123.2*	2.02	1.91	1.91	(17,11)
57.6	27.6	27.3	R	149.3*	1.66	1.69	1.63	(13,11)
56.6	33.4	33.4	L	126.7*	1.96	1.83	1.97	(13,16)
27.3	2.7	2.7	R	169.8*	1.46	---	1.45	(18,1)

[a]The * in red and blue colors indicate that the excitation lasers are 632.8 and 514.5 nm, respectively.

= $\varphi_R' - 30°$). Similarly, to a L-SWNT in the blue area in Figure 4d, such as (2,7)-L, the chiral angle θ ranges from 30 to 60°. If the graphene trench appears along the ZZ_3 (ZZ_4) edges, and the formed angle with the SWNT axis is φ_L (φ_L'), the chiral angle of L-SWNT is logically $\theta = 30° + \varphi_L$ ($\theta = 90° - \varphi_L'$). Moreover, if the angle φ between the SWNT axis and the graphene trench is larger than 60°, such as φ_R'' and φ_L'', they can be reduced into 0° − 60° by $\varphi = |\varphi'' - i \times 60°|$ (i is an integer here) due to the D_{6h} symmetry of graphene lattice. In this way, the chiral angle of SWNTs can be exactly calculated by the angle between SWNT and the graphene trench. The approaches to handedness and chiral angle characterization are mathematically summarized in Table 1.

Experimentally, the SWNTs were grown following the kite-flying mechanism[34] (see Figure S2 in Supporting Information). As shown in the scanning electron microscopy (SEM) image in Figure 5b, two ultralong SWNTs simultaneously fell onto the same graphite surface. Graphite trenches were randomly appeared and exactly along ZZ directions in the STM image with atomic resolution (see Figure S3 in Supporting Information). Figure 5c–f demonstrated detailed characterizations of the handednesses and chiral angles of aligned SWNTs on a graphite surface. The SWNTs in Figure 5c are grown along two directions with the formed angle of 120°, which corresponds to the D_{6h} symmetry of graphene. The linear graphene trench appears in the counter-clockwise direction of SWNT, and their angle is $\varphi = \varphi'' - 60° = 74.8° - 60° = 14.8°$; thus, the SWNT is right-handed, with $\theta = 30° - \varphi_R = 30° - 14.8° = 15.2°$. Similarly, the graphene trench in Figure 5d is in the clockwise direction of SWNT, and their formed angle is 62.1° (2.1°); therefore, this SWNT is left-handed, with $\theta = 30° + \varphi_L = 30° + 2.1° = 32.1°$. In Figure 5e,f, the angles between SWNTs and the graphene trenches are only 30.0° and 60.0°; thus, they are ZZ-SWNT with $\theta = 0°$, and AC-SWNT with $\theta = 30°$, respectively.

In order to further assign (n,m) indices of as-grown SWNTs, the determination of diameter is quite crucial to the (θ,d) plot. Many reports prove that the AFM technique is suitable for the grown SWNTs with $d < 2.2$ nm.[35] Moreover, the graphite with an atomically smooth surface is amenable to diameter measurement with a smaller roughness than Si (see Figure S4 in Supporting Information). Additionally, the RBM peak of SWNT has already been widely used to speculate its diameter due to $d = c/\omega_{RBM}$ (the constant c is 248.3 nm/cm^{-1} for as-grown SWNTs on the SiO_x/Si surface[36]). In Figure 6a, the SWNT on a graphite surface is left-handed with chiral angle θ = 39.9° and diameter d = 1.68 nm by AFM. At 632.8 nm excitation, the RBM peak of 154.4 cm^{-1} indicates that the SWNT is semiconducting with diameter of 1.61 nm. Therefore, we can easily and uniquely confirm that (39.9°, 1.61 nm) corresponds to the (8,15)-L-S SWNT from the partial (θ,d) plot in Figure 6c. In this way, the chiral indices of aligned SWNTs on graphite can be directly and exactly obtained from the AFM image.

The (θ,E_{ii}) plot for chiral index assignment demands the chiral angle and electron transition energy of SWNT. According to resonant Raman scattering theory, the transition energy E_{ii} of isolated SWNT can be accurately determined by the anti-Stokes/Stokes resonant Raman intensity ratio, and the precision is better than 5 meV.[37,38] In Figure 6d, the SWNT on a graphite surface is right-handed with chiral angle θ = 22.7° and diameter d = 1.91 nm, so the chiral index is (17,11)-R-M from (θ,d) plot. At 514.5 nm excitation, the RBM peak of 123.2 nm indicates that the SWNT is metallic, and the intensity ratio of the anti-Stokes/Stokes Raman shift is 2.66, as shown in Figure 6e, which means that the transition energy E_{22} of this SWNT is 2.415 eV (see Figure S5 in Supporting Information). Therefore, the chiral index can also be assigned to (17,11)-R-M from the corresponding (θ,E_{22}) plot in Figure 6f. Importantly, the obtained chiral indices of SWNT from the (θ,d) plot and (θ,E_{ii}) plot are identical, which illustrates that these characterization approaches are both accurate and reliable.

The quick and accurate approach through the (θ,d) plot is advantageous to the chiral structure determination of extensive SWNTs on a large scale. Table 2 displays several measured SWNTs with comprehensive chiral structures. By comparing the experimental and calculated chiral angle, the accuracy of the measured chiral angle is better than 0.3°, which is precise enough for handedness determination. In addition, the diameters obtained by AFM present a greater fluctuation than that by RBM peaks due to the instable interactions between SWNTs and AFM tips. Even so, the chiral index of SWNT can be uniquely identified from the (θ,d) plot by combining the measured chiral angle and diameter.

In summary, a novel strategy was put forward to comprehensively determine the chiral structures of SWNTs, including handedness, chiral angle, and chiral index, by aligning the SWNTs on graphite surface with chirality-dependent orientations. Taking the graphite trenches with ZZ edges as necessary references, detailed formulas were summarized, and they are much more suitable to determine the handedness and chiral angle of grown SWNTs on graphite. Moreover, by combining the measured diameter and electron transition energy of SWNTs, the chiral index of SWNTs were rapidly and accurately identified from the useful (θ,d) and (θ,E_{ii}) plots, respectively. This universal strategy provides efficient and convenient approaches to chiral structure determination on a large scale, and it represents an important step forward in the characterization methodology of SWNTs.

■ ASSOCIATED CONTENT

Supporting Information

Experimental details and supplementary figures. This material is available free of charge via the Internet at http://pubs.acs.org.

dx.doi.org/10.1021/nl403336x | Nano Lett. 2013, 13, 5666–5671

AUTHOR INFORMATION

Corresponding Author

*E-mail: jinzhang@pku.edu.cn. Tel/Fax: 86-10-6275-7157.

Notes

The authors declare no competing financial interest.

ACKNOWLEDGMENTS

The authors are very grateful to Professor Pingheng Tan (Institute of Semiconductors, Chinese Academy of Sciences, China) and Professor Qingming Zhang (Renmin University of China) for their help with Raman measurements. This work was supported by NSFC (21233001, 21129001, 51272006 and 51121091) and MOST (2011CB932601).

REFERENCES

(1) Iijima, S. *Nature* **1991**, *354*, 56−58.
(2) Novoselov, K. S.; Geim, A. K.; Morozov, S. V.; Jiang, D.; Zhang, Y.; Dubonos, S. V.; Grigorieva, I. V.; Firsov, A. A. *Science* **2004**, *306*, 666−669.
(3) Iijima, S.; Ichihashi, T. *Nature* **1993**, *363*, 603−605.
(4) Ilani, S.; McEuen, P. L. *Annu. Rev. Condens. Matter Phys.* **2010**, *1*, 1−25.
(5) Tans, S. J.; Verschueren, A. R. M.; Dekker, C. *Nature* **1998**, *393*, 49−52.
(6) Avouris, P.; Freitag, M.; Perebeinos, V. *Nat. Photonics* **2008**, *2*, 341−350.
(7) Baughman, R. H.; Zakhidov, A. A.; de Heer, W. A. *Science* **2002**, *297*, 787−792.
(8) Behabtu, N.; Young, C. C.; Tsentalovich, D. E.; Kleinerman, O.; Wang, X.; Ma, A. W. K.; Bengio, E. A.; ter Waarbeek, R. F.; de Jong, J. J.; Hoogerwerf, R. E.; Fairchild, S. B.; Ferguson, J. B.; Maruyama, B.; Kono, J.; Talmon, Y.; Cohen, Y.; Otto, M. J.; Pasquali, M. *Science* **2013**, *339*, 182−186.
(9) De Volder, M. F. L.; Tawfick, S. H.; Baughman, R. H.; Hart, A. J. *Science* **2013**, *339*, 535−539.
(10) Xie, L. M.; Wang, H. L.; Jin, C. H.; Wang, X. R.; Jiao, L. Y.; Suenaga, K.; Dai, H. J. *J. Am. Chem. Soc.* **2011**, *133*, 10394−10397.
(11) Dresselhaus, M.; Dresselhaus, G.; Jorio, A. *Annu. Rev. Mater. Res.* **2004**, *34*, 247−278.
(12) Chiang, W. H.; Sankaran, R. M. *Nat. Mater.* **2009**, *8*, 882−886.
(13) He, M. S.; Jiang, H.; Liu, B.; Fedotov, P. V.; Chernov, A. I.; Obraztsova, E. D.; Cavalca, F.; Wagner, J. B.; Hansen, T. W.; Anoshkin, I. V. *Sci. Rep.* **2013**, *3*, 1460−1467.
(14) Rao, R.; Liptak, D.; Cherukuri, T.; Yakobson, B. I.; Maruyama, B. *Nat. Mater.* **2012**, *11*, 213−216.
(15) Chen, Y. B.; Hu, Y.; Fang, Y.; Li, P.; Feng, C. Q.; Zhang, J. *Carbon* **2012**, *50*, 3295−3297.
(16) Foroughi, J.; Spinks, G. M.; Wallace, G. G.; Oh, J.; Kozlov, M. E.; Fang, S. L.; Mirfakhrai, T.; Madden, J. D. W.; Shin, M. K.; Kim, S. J.; Baughman, R. H. *Science* **2011**, *334*, 494−497.
(17) Odom, T. W.; Huang, J. L.; Kim, P.; Lieber, C. M. *Nature* **1998**, *391*, 62−64.
(18) Wildoer, J. W. G.; Venema, L. C.; Rinzler, A. G.; Smalley, R. E.; Dekker, C. *Nature* **1998**, *391*, 59−62.
(19) Yoshida, H.; Takeda, S.; Uchiyama, T.; Kohno, H.; Homma, Y. *Nano Lett.* **2008**, *8*, 2082−2086.
(20) Warner, J. H.; Young, N. P.; Kirkland, A. I.; Briggs, G. A. D. *Nat. Mater.* **2011**, *10*, 958−962.
(21) Allen, C. S.; Zhang, C.; Burnell, G.; Brown, A. P.; Robertson, J.; Hickey, B. J. *Carbon* **2011**, *49*, 4961−4971.
(22) Kataura, H.; Kumazawa, Y.; Maniwa, Y.; Umezu, I.; Suzuki, S.; Ohtsuka, Y.; Achiba, Y. *Synth. Met.* **1999**, *103*, 2555−2558.
(23) Dresselhaus, M. S.; Dresselhaus, G.; Saito, R.; Jorio, A. *Phys. Rep.* **2005**, *409*, 47−99.
(24) O'Connell, M. J.; Bachilo, S. M.; Huffman, C. B.; Moore, V. C.; Strano, M. S.; Haroz, E. H.; Rialon, K. L.; Boul, P. J.; Noon, W. H.; Kittrell, C.; Ma, J. P.; Hauge, R. H.; Weisman, R. B.; Smalley, R. E. *Science* **2002**, *297*, 593−596.
(25) Bachilo, S. M.; Strano, M. S.; Kittrell, C.; Hauge, R. H.; Smalley, R. E.; Weisman, R. B. *Science* **2002**, *298*, 2361−2366.
(26) Sfeir, M. Y.; Wang, F.; Huang, L. M.; Chuang, C. C.; Hone, J.; O'Brien, S. P.; Heinz, T. F.; Brus, L. E. *Science* **2004**, *306*, 1540−1543.
(27) Hunley, D. P.; Johnson, S. L.; Stieha, J. K.; Sundararajan, A.; Meacham, A. T.; Ivanov, I. N.; Strachan, D. R. *ACS Nano* **2011**, *5*, 6403−6409.
(28) Falvo, M. R.; Steele, J.; Taylor, R. M.; Superfine, R. *Phys. Rev. B* **2000**, *62*, 10665−10667.
(29) Ortolani, L.; Houdellier, F.; Monthioux, M.; Morandi, V. *Carbon* **2010**, *48*, 3050−3056.
(30) Chen, Y. B.; Shen, Z. W.; Xu, Z. W.; Hu, Y.; Xu, H. T.; Wang, S.; Guo, X. L.; Zhang, Y. F.; Peng, L. M.; Ding, F.; Liu, Z. F.; Zhang, J. *Nat. Commun.* **2013**, *4*, 2205−2230.
(31) Samsonidze, G. G.; Gruneis, A.; Saito, R.; Jorio, A.; Souza, A. G.; Dresselhaus, G.; Dresselhaus, M. S. *Phys. Rev. B* **2004**, *69*, 205402−205412.
(32) Shi, Z. W.; Yang, R.; Zhang, L. C.; Wang, Y.; Liu, D. H.; Shi, D. X.; Wang, E. G.; Zhang, G. Y. *Adv. Mater.* **2011**, *23*, 3061−3065.
(33) Ci, L. J.; Song, L.; Jariwala, D.; Elias, A. L.; Gao, W.; Terrones, M.; Ajayan, P. M. *Adv. Mater.* **2009**, *21*, 4487−4491.
(34) Huang, S. M.; Maynor, B.; Cai, X. Y.; Liu, J. *Adv. Mater.* **2003**, *15*, 1651−1655.
(35) Alizadegan, R.; Liao, A. D.; Xiong, F.; Pop, E.; Hsia, K. J. *Nano Res.* **2012**, *5*, 235−247.
(36) Jorio, A.; Saito, R.; Hafner, J. H.; Lieber, C. M.; Hunter, M.; McClure, T.; Dresselhaus, G.; Dresselhaus, M. S. *Phys. Rev. Lett.* **2001**, *86*, 1118−1121.
(37) Souza, A. G.; Jorio, A.; Hafner, J. H.; Lieber, C. M.; Saito, R.; Pimenta, M. A.; Dresselhaus, G.; Dresselhaus, M. S. *Phys. Rev. B* **2001**, *63*, 241404R−241407R.
(38) Jorio, A.; Souza, A. G.; Dresselhaus, G.; Dresselhaus, M. S.; Saito, R.; Hafner, J. H.; Lieber, C. M.; Matinaga, F. M.; Dantas, M. S. S.; Pimenta, M. A. *Phys. Rev. B* **2001**, *63*, 245416−245419.